RSC Advances

ROYAL SOCIETY OF CHEMISTRY

www.rsc.org/advances

Journal Name

ARTICLE

Size effects of alkylimidazolium cations on the interfacial properties and CO_2 uptake capacity in layered organic-inorganic imidazolium-TiO_2 hybrids

Received 00th January 20xx,
Accepted 00th January 20xx

DOI: 10.1039/x0xx00000x

www.rsc.org/

He Liu, Haitao Zhang*, Peng Shen, Guoying Zhao, Suojiang Zhang*

Layered inorganic-organic TiO_2-ILs hybrids with tunable basal spacing were fabricated through electrostatic interaction between 2D inorganic nanosheets and organic imidazolium-based ILs. Imidazolium cations with various sizes were intercalated into lamellar titanate nanosheets, forming layered structures with slabs turbostratic restacking. The effects of cation sizes on the interfacial properties of hybrids were comprehensively investigated by XRD, SEM, TEM, AFM, FT-IR, Raman and TG techniques. The results confirmed that the ratio of interlayer imidazolium cations declined with the increase of carbon chain length. A CO_2 absorption experiment was conducted and TiO_2-ILs compounds displayed enhanced CO_2 absorption capacity with the increase of alkyl chain length, which could be attributed to the synergistically interfacial effects induced by the diverse interactions between ILs and inorganic nanosheets. An absorption mechanism was proposed on account of the ion-exchangeable characteristic of these layered hybrids and the intercalated H_2O molecules were found to play a crucial role in CO_2 uptake.

1. Introduction

CO_2 capture and storage (CCS) is a hot and challenging research topic for environmental concerns.[1-4] Enormous porous solids, such as porous carbon,[5-9] zeolites,[10-12] MOFs/ZIFs,[13-19] and other functional polymers,[20-23] have been intensively exploited as CO_2 gas adsorbents. The crystal size of these porous materials could be reduced in order to enhance the gas adsorption/desorption kinetics. However, the complexity in pore structures and difficulty in controlling the size and chemical nature of pores lead to the starvation of CO_2 in the inner pores and further a low utilization of the overall surfaces and porosities, thus extending the time for CO_2 molecules to transfer into and out of the inner microporous networks.[24] To address this issue, two-dimensional (2D) inorganic nanosheets have been proposed as promising building blocks to form porous and highly active hybrids for CO_2 adsorption owing to their high surface area and abundant accessible active sites.[24-30] Their open pore structures, arising from the stacking of monoatomic layer nanosheets, favor fast sorption kinetics. In addition, exfoliation-reassembling strategy enables intercalation of diverse guest species within the host lattice, thus providing much greater flexibility in tailoring the pore size and chemical bonding nature of the pore walls within the resulting hybrid materials.[28] However, the insufficient adsorption capacity and poor stability hinder their practical applications.[31] Thus, the fabrication of novel nanoarchitectures based on the hybridization of inorganic 2D nanosheets with enhanced CO_2 uptake capacity and stability is greatly desired.[32]

Separating CO_2 from industrial gases by ionic liquids (ILs) is an emerging capture technology.[33-37] Many attentions have been paid on the absorption of CO_2 by using imidazolium-type ILs, as they are commercially available and chemically tunable.[38-41] Generally, anions in ILs are the dominant factors for gas solubility and the length of alkyl chain in alkylimidazolium cations acts a critical role in the diffusion behaviour of CO_2 molecules.[42, 43] Immobilizing a thin film of ILs onto a support with high surface area can not only minimize the amount of utilized ILs on the basis of economic criteria and possible toxicological concerns, but also reduce the mass transfer limitations induced by high viscosity of ILs.[44] Furthermore, immobilization could combine the advantages of ILs with those of support materials.[45] The intrinsic organization and physicochemical properties of ILs influence the construction of solid host network. Conversely, confinement effects can modify properties of the guest ILs.[46]

The interfacial interactions between ILs and supports are vitally important, as the physicochemical properties of the composites can be decided by the interactions.[47, 48] Recently, ILs properties at the interface with carbon-based electrodes are of great concern, since the stability of the composites at charged interfaces has a decisive effect on electrochemical applications.[49] The studies on the interfacial properties between ILs and mesoporous TiO_2 surfaces demonstrated that the wetting behaviour of ILs on TiO_2 films influences the rate of CO_2 adsorption.[50] To obtain a high specific interface area in hybrid systems, one reliable approach is to disperse ILs onto the 2D nanosheets.[51] The ultrathin thickness and

Beijing Key Laboratory of Ionic Liquids Clean Process, Key Laboratory of Green Process and Engineering, State Key Laboratory of Multiphase Complex Systems, Institute of Process Engineering, Chinese Academy of Sciences, Beijing 100190, PR China

† Footnotes relating to the title and/or authors should appear here.
Electronic Supplementary Information (ESI) available. See
DOI: 10.1039/x0xx00000x

extremely large surface of 2D nanosheets render them achieving a strong coupling with ILs and maximizing the effect of hybridization on the physicochemical properties and functionality of hybridized components. TiO_2 nanosheets are promising precursors for creating novel mesoporous adsorbents by restacking them in the presence of organic or inorganic compounds, which can pillar within the interlayered space.[28, 29, 52] The nanohybrids of layered titanate pillared with basic metal oxide nanoclusters can capture CO_2 with improved efficiency and thermal stability.[28] Therefore, it is of great value to fabricate layered organic-inorganic hybrids composed of 2D TiO_2 nanosheets and imidazolium-based ILs and investigate their performance in absorbing CO_2.

Herein, four kinds of imidazolium-based ILs with various carbon chain lengths in alkylimidazolium cations were hybridized with TiO_2 nanosheets *via* an exfoliation-restacking process to fabricate layered TiO_2-ILs hybrids. The CO_2 adsorption tests were conducted to investigate the interfacial effects on the performance of CO_2 uptake.

2. Experimental Section

2.1 Reagents and Materials

Titanium dioxide (rutile form, 99.5 %) from Alfa Aesar and Cs_2CO_3 (99.9 %) from Aladdin were used as received for the synthesis of layered titanate crystals. Tetrabutylammonium hydroxide (TBA·OH hereafter) aqueous solution (40 wt %) from J&K Co., were used as received. Ionic liquids (99 %) were purchased from Linzhou Keneng Materials Technology Co. and used as received. Other reagents were of analytical grade. Ultra-pure water (18.2 mΩ) was used throughout the study.

2.2 Synthesis of titanate nanosheets

Exfoliated TiO_2 nanosheets were achieved *via* a proton-exchange and osmotic swelling process.[53-55] A mixture of TiO_2, Cs_2CO_3 was heated in air at 800 ℃ for 10 h to form cesium titanate $Cs_{0.7}Ti_{1.825}\square_{0.175}O_4$ (□ = vacancy). Its acid-exchanged layered precursor of $H_{0.7}Ti_{1.825}\square_{0.175}O_4{\cdot}H_2O$ (HTO hereafter) was delaminated into its molecular single sheets through mechanical shake with the presence of organic amines TBA·OH, producing a stable titanate nanosheet colloidal suspension of $Ti_{1-\delta}O_2^{4\delta-}$ ($\delta \sim 0.09$). The freeze-dried products were denoted as TiO_2-TBA. Flocculated TiO_2 was obtained by adding HCl solution (1 M) into colloidal nanosheet solution and collected by centrifugation (referred as TiO_2-H^+).

2.3 Intercalation of ILs into titanate layers

The as-prepared titanate nanosheets were assemblied with four kinds of imidazolium ILs with different carbon chain length in imidazolium cations: 1-ethyl-3-methylimidazolium chloride (EmimCl), 1-butyl-3-methylimidazolium chloride (BmimCl), 1-hexyl-3-methylimidazolium chloride (HmimCl) and 1-octyl-3-methylimidazoliumchloride (OmimCl). Typically, 2 g of OmimCl was added to 200 mL of titanate nanosheet colloidal suspension (2.5 g L^{-1}) under constant stirring, immediately resulting in flocculent precipitates. After stirring for several hours, the solid product was separated from the suspension by centrifugation and redispersed in 200 mL of deionized water. Repeated the process for 5 - 6 times to promote a complete ion-exchange between imidazolium cations and interlayer TBA^+. Finally, the precipitates were filtered, washed thoroughly with deionized water and dried by freeze-drying, forming cottonlike ILs-entrapped TiO_2 hybrid gels.

The assembling of TiO_2 nanosheets with EmimCl, BmimCl and HmimCl were similar to the process mention above, except that the amounts of ILs in use were different. Generally, imidazolium-based ILs with longer carbon chains were less consumed. On the basis of Schulze-Hardy rule, the coagulation ability of cations with the same valence state enhances with the increase of ionic radius, as the larger cation radius accompany with lower hydration ability and higher absorption capacity on colloid particles. Thus imidazolium cations with longer alkyl chains have stronger interactions with titanate nanosheets, leading to easier substitution of TBA^+ cations and less consumption of ILs. In another respect, long alkyl chains tended to bend and twine together, accelerating the aggregation of nanosheets. As-prepared TiO_2-ILs hybrids were referred as TiO_2-Xmim (X = E, B, H, O, respectively).

2.4 Characterizations

Crystal structure was analyzed by an X-ray diffractometer (XRD, Rigaku, Smartlab) equipped with a Cu $K_{\alpha1}$ radiation source (9 kW, λ = 0.15406 nm) and a 1D silicon strip detector (D/teX Ultra 250). The morphologies and microstructures were investigated by a transmission electron microscopy (TEM, JEOL-2010) with an accelerating voltage of 200 kV, and a scanning electron microscopy (SEM, JEOL JSM-7001F). Atomic force microscopy (AFM) images were collected on a Nanoscale IIIA (Digital Instrument) in a taping mode with a silicon tip cantilever (force constant: 20 mN m^{-1}); the silicon substrates used for depositing the nanosheets were pretreated with the PDDA solution. Fourier transform infrared (FTIR) data were recorded on a Thermo Nicolet 380 spectroscopy. The Raman spectra were recorded by a microspectrometer (LabRAM HR800, Horiba Jobin-Yvon) with an excitation laser at 514 nm. Thermogravimetric analysis (TGA) was performed on a thermogravimetry/differential thermal analyzer (STA7200RV, Hitachi High-Tech) at a heating rate of 10 $^oC\ min^{-1}$.

The evaluation of CO_2 uptake capacity of the samples was conducted on an Intelligent Gravimetric Analyser (IGA-100A, HIDEN). Typically, 10 - 15mg of samples were placed in a quartz basket, and pretreated in vacuum at 50 ^oC for 12 h to remove surface absorbed moisture and impurities. Then CO_2 uptake amounts were recorded at 25 ^oC at the pressure of 100, 200, 300, 400, 500, 700, 1000, 1500, 2000, 3000 and 4000 mbar, respectively. Every pressure point was kept for 30 - 300 min to reach the adsorption equilibration. Adsorption equilibration criteria of every pressure point were set as the 95 % percentage of saturated adsorption capacity, which was a simulated value of asymptotic uptake.

3. Results and discussion

The structure of layered protonic titanate (HTO) is orthorhombic (space group Immm) and consists of 2D TiO_6 octahedral host layers and interlayer water molecules (H_2O and/or H_3O^+).[56, 57] The neighboring TiO_6 octahedral host layers are held together by hydrogen bonding between the interlayer water molecules and the 2-coordinated oxygens.[57] The freeze-dried exfoliated titanate

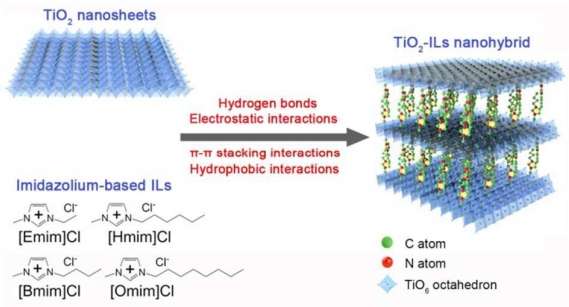

Scheme 1. Formation schemes of TiO_2/ILs nanocomposites.

nanosheets (TiO_2-TBA) are lamellar aggregates reassembled by 10-20 titanate nanosheets accommodating with TBA^+ cations and water molecules in the interspace of 2D TiO_6 host layers.[54] The hybridization of ILs with titanate nanosheets is a process of ion-exchange between imidazolium cations and interlayer TBA^+/water molecules. As access amounts of ILs were added to the colloidal suspension, and the ion-exchange process was repeated for 5 times, the TBA^+ cations are completely substituted. As a result, only some water molecules are left in the interlayer, since hydrogen bonding between the interlayer water molecules and O atom on the slabs makes it difficult to replace H_2O and/or H_3O^+. Consequently, the chemical reactions of the hybridization process are summarized and expressed in Equation 1.

$$TiO_2\text{-TBA}/H_3O^+ + BmimCl \rightarrow TiO_2\text{-Bmim}/H_3O^+ + HCl + TBACl \quad \text{(Equation 1)}$$

The layered organic-inorganic imidazolium-TiO_2 hybrids obtained through an exfoliated-restacking process are illustrated in Scheme 1. The composites could be formed by the electrostatic interactions between positive imidazolium and negative nanosheets through bridging O atoms in TiO_6 octahedron. A thin layer of imidazolium ions was attached onto titanate surface through π-π stacking interactions between the neighboring imidazolium cations.[58] Moreover, hydrogen bonds formed between H atom at position-2 of imidazolium ring (C_2-H) and O atom on the slabs,[58] as well as hydrophobic interactions between the carbon chains of adjacent imidazolium cations,[59] served as strong driving forces in binding host layers with ILs. Therefore, turbostratic stacking of sheet-like crystallites was attained through this hybridization process. Restacking of 2D crystallites can form mesopores in the interlayer space, and intercalation of ILs favor the formation of micropores. Such a hierarchical porous structure is quite effective for improving the adsorptive and catalytic activity of hybrid materials.[60]

XRD technique was used to monitor the crystal evolution in the exfoliation and restacking processes. All diffraction peaks in protonic titanate precursor HTO can be readily indexed on the basis of a body-centered orthorhombic structure (space group *Immm*).[61] The diffraction peak at 2θ of ~ 5° was characteristic of layered or sheet-like structures.[62] The sharp peak at 2θ of 8.8° in TiO_2-H^+ was assignable to (010) reflections with a *d*-spacing of 1.00 nm.[57] In ILs-entrapped TiO_2 hybrids, the decrease of peak intensity and peak sharpness suggested a decline in the layer-by-layer ordering of the intercalation phase.[57] The basal spacings of (010) reflections varied to 1.72, 2.34, 1.52 and 1.77 nm for TiO_2-Emim, TiO_2-Bmim, TiO_2-Hmim and TiO_2-Omim, respectively (Fig. 1d - g). Considering that the intrinsic thickness of titanate monolayer is 0.7 nm, [56, 63] the

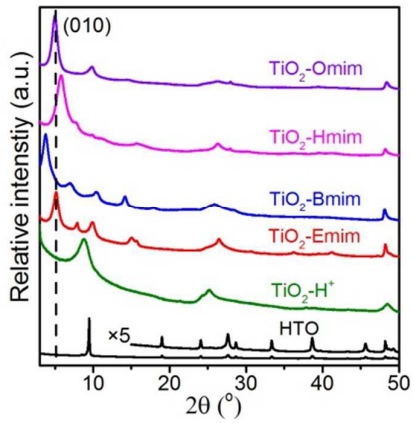

Fig.1 XRD patterns of exfoliated TiO_2 nanosheets and TiO_2-ILs nanocomposites.

corresponding gallery heights of observed basal spacing were 1.02, 1.64, 0.82 and 1.07 nm, respectively. Gallery height of the hybrids should be logically positive correlation with the size of interlayer cations. The expanding basal spacings of TiO_2-ILs hybrids implied the validity of intercalating ILs in the interlayer space of layered titanate, as ILs has a larger size than of H_3O^+. In TiO_2-ILs hybrids, gallery height increases with the length of alkyl chain in imidazolium cations, if alkyl chain is straight and perpendicular to the TiO_6 host slabs as illustrated in Scheme 1. Thus the intersheet distance of TiO_2-Bmim was larger than that of TiO_2-Emim. The values of these two hybrids were larger than the theoretically maximum length of their corresponding imidazolium cations obtained by DFT method (Table 1), resulting from the surface adsorption of water molecules on nanosheets. Actually, variations in intersheet distance were also influenced by the arrangement orientation of carbon chains in the interlayer region.[64] The gallery heights of TiO_2-Hmim and TiO_2-Omim were less than that of TiO_2-Bmim, indicating that the alkyl chains in the former two possibly lay on the interspace of nanosheets and arranged parallel to the laminar structures, as the longer carbon chains tended to bend and twine together. This was confirmed by the theoretically maximum lengths of $Hmim^+$ and $Omim^+$ cations in Table 1, which were longer than the interlayer height of TiO_2-Hmim and TiO_2-Omim. The swelling and the basal spacing of layered materials depends on the ratio of repulsive potential, and the difference of size in the interlayer cations may affect the repulsive potential and attractive force of the neighbouring titanate sheets.[65] Thus, it may also reflect the strength changes in the electrostatic interactions and hydrogen bonds between the hybridized components.

The morphology of TiO_2 nanosheets and TiO_2-ILs nanocomposites was investigated by microscopes. Fig. 2 shows the SEM images of TiO_2 nanosheets and TiO_2-ILs nanocomposites. Typical SEM images of the freeze dried nanosheets (Fig. 2a) revealed clearly the plate-like morphology of the resulting nanosheets with a lateral size of several to tens of microns. These results lead to the conclusion that the exfoliated nanosheets restacked together forming layered structures upon freeze-drying.[66] Flocculated TiO_2 with HCl solution showed layered structures with curled characteristic in the edge, leading to more spaces between

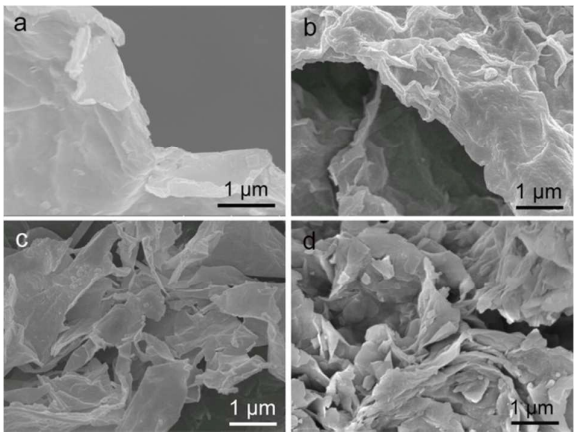

Fig. 2 SEM images of a) exfoliated TiO_2 nanosheets, b) TiO_2-H^+, c) TiO_2-Bmim, and d) TiO_2-Omim hybrids.

slices (Fig. 2b). The imidazolium rings were confined within the gallery of restacking layered materials upon ion-exchange. The hybrids kept the basic plate-like morphology of titanate slabs with some extent of agglomeration. SEM image of TiO_2-Bmim exhibited lamellar structures with nanosheets turbostratic restacking (Fig. 2c), while slices in TiO_2-Omim were agglutinating more severely (Fig. 2d), resulting from the bending and winding characteristics of long alkyl chains in imidazolium cations and stronger electrostatic forces and hydrophobic interactions within carbon chains.

AFM observation revealed that the exfoliated nanosheet was with a thickness of ca. 1.71 nm and lateral size of ~100-600 nm (Fig. 3a). The larger thickness of exfoliated nanosheets obtained by AFM than the crystallographic thickness of the host layer (0.7 nm)[56, 63] was ascribed to surface adsorption of solvents (water molecule) or guest species on nanosheets.[67] TEM image of TiO_2-H^+ (Fig. 3b) exhibited layered structures with some curls in the edge of the slabs, in accordance with the SEM image. In contrast, the nanocomposites hybridized with ILs (Figure 3c, d) exhibited house-of-cards-type stacking structure of sheet-like crystallites with more channels between the slices, indicating the incorporation of ILs into the interlayer space of TiO_2 nanosheets. Additionally, TiO_2-Bmim showed vaguer morphology than that of TiO_2-Hmim, which might be due to the surrounding of excess organic BmimCl molecules.

The FT-IR spectra of the TBA- and Bmim-intercalated titanate (Fig. 4) showed different absorption bands. Vibrational spectrum of TiO_2-TBA (Fig. 4a) confirmed that TBA^+ ions and H_2O species were trapped in the lattice.[54] The bands at round 700-500 cm^{-1} were attributed to Ti-O stretching vibrations.[68] The broad band at about 3420 cm^{-1} and a prominent absorption at 1635 cm^{-1} were ascribed to stretching and bending vibrations of H_2O, respectively.[56] The peaks at 2960 - 2873 cm^{-1} and 1465 - 1382 cm^{-1} belonged to stretching and bending vibrations of C-H, respectively, and peaks at 1100 - 1000 cm^{-1} were assigned to C-N stretching vibrations in TBA^+ cations.[68] Upon ion-exchange with $Bmim^+$, the absorption bands for C-H and C-N vibrations were observed (Fig. 4b), as these structures existed in $Bmim^+$ cations. In addition, new vibrations at 1474 cm^{-1} belonged to C=C bonds in imidazolium rings and absorptions at 963 cm^{-1}, 888 cm^{-1} and 787 cm^{-1} were assigned to bending vibrations of C-H in unsaturated carbons in $Bmim^+$,[69] indicating the successful substitution of $Bmim^+$ into the 2D host layers.

Raman spectra of pristine titanate and their ion-exchangeable counterparts were collected to investigate the effects of substituted

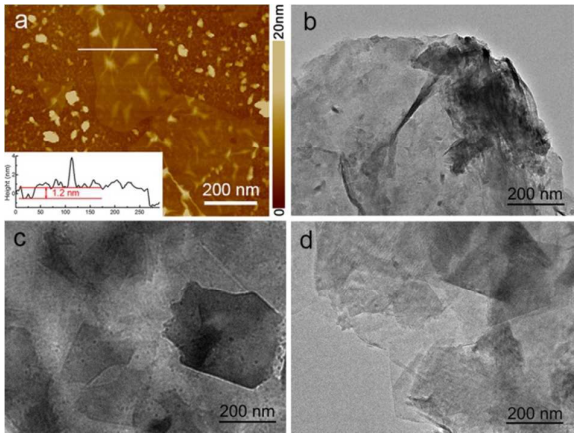

Fig. 3 a) AFM image of exfoliated TiO_2 nanosheets and TEM images of b) TiO_2-H^+, c) TiO_2-Bmim, and d) TiO_2-Omim.

Table 1. The interlayer spacing of TiO_2-ILs hybrids and ratio of interlayer species to TiO_2 host framework in hybrids.

Sample name	Interlayer species	Basal spacing (nm)[a]	Gallery height (nm)[a]	Length of cations (nm)[b]	Molar ratio/TiO_2[c]	
					H_3O^+	Cations
TiO_2-H^+	H_3O^+	1.00	0.30	-	0.95	-
TiO_2-Emim	$Emim^+$	1.72	1.02	0.85	0.77	0.46
TiO_2-Bmim	$Bmim^+$	2.34	1.64	0.98	0.27	0.20
TiO_2-Hmim	$Hmim^+$	1.52	0.82	1.32	0.31	0.14
TiO_2-Omim	$Omim^+$	1.77	1.07	1.55	0.41	0.15

[a] calculated from XRD analysis;
[b] optimized structures of imidazolium cations by DFT method;
[c, d] the molar ratio of interlayer species to the TiO_2 host framework calculated from TGA curves.

Journal Name

ARTICLE

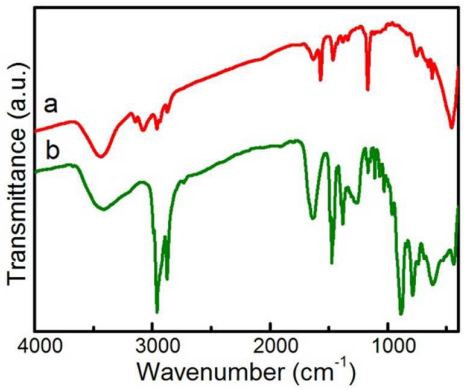

Fig. 4 FT-IR spectra of a) TBA- and b) Bmim-intercalated titanate.

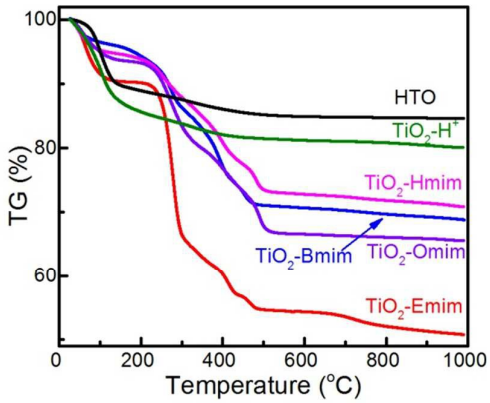

Fig. 6 TGA curves of TiO_2 nanosheets and TiO_2-ILs nanohybrids.

imidazolium cations on the structure evolution of composites. As plotted in Fig. 5, nine Raman bands (186, 271, 386, 450, 558, 658, 702, 816, and 911 cm^{-1}) at 100 - 1000cm^{-1} spectral region in layered HTO precursor were attributed to the Ti-O lattice vibrations within 2D lepidocrocite-type TiO_6 octahedral host layers.[57] This Raman spectrum of TiO_2-H^+ was similar to that of the layered titanate precursor, implying the main framework with H^+ cations locating between the slices remained unchanged., The intensity of bands assigned for Ti-O vibrations in the spectra of TiO_2-ILs hybrids changed mildly, while new bands at 772, 928 and 1024cm^{-1} were correlated to the vibrations of the bonds in imidazolium rings.[70] The band at 186 cm^{-1} could be ascribed to an external vibration that derives from the translational motion of the 2D TiO_6 octahedral host layers, and variation intensity was correlated with the nature of the interlayer species.[57] Moreover, Raman variation at 271 and

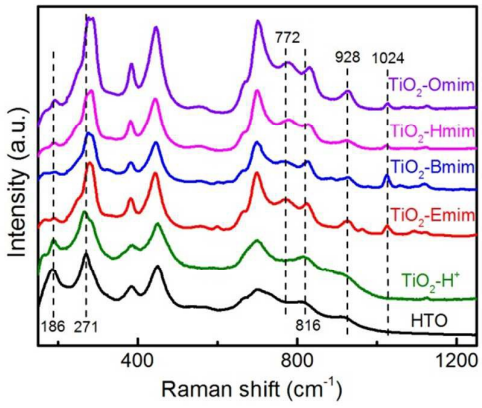

Fig. 5 Raman spectra of TiO_2 nanosheets and TiO_2-ILs nanohybrids.

816 cm^{-1} shifted to higher wavenumber, implying that the substituted imidazolium cations modified the skeletal vibrations of TiO_6. All these results reconfirmed that H^+ ions in the gallery were replaced by imidazolium cations, and the incorporated imidazolium cations were successfully bound with the TiO_2 host layers.

TGA curves (Fig. 6) were collected to assess the content of the ILs and water inside the layered titanate, and the temperature range for weight loss of interlayer species can be directly observed from the DTG curves in Fig. 7. Two distinguished weight loss regions at 40 - 200 °C (step I) and 200 - 500 °C (step II) were observed in TiO_2-H^+ (Fig. 7a). These layered compounds lost interlayer water molecule firstly in step I, resulting into a dehydrated phase, and then underwent complete dehydration to form the final anatase (step II).[71] TiO_2-H^+ exhibited the highest thermal stability with a weight loss of 12 % at 200 °C, confirming that the interlayer space were occupied by water molecules. Decomposition of TiO_2-ILs compounds took place mainly in four temperature regions at *ca.* 40 - 200, 220 - 310, 310 - 450 and 450 - 500 °C (Fig. 7b). The second weight loss corresponded to the degradation of ILs adsorbed on the surface of layered titanate, as neat BmimCl was completely decomposed before 310 °C.[64] TiO_2-Emim underwent large weight loss at this region, implying that excess $Emim^+$ cations were attached on the surface and edge region of the composites.[72] The third weight loss can be assigned to the degradation of intercalated ILs in the gallery. The delayed degradation of ILs was due to the protection of inorganic layers, as ILs were confined in the interlayer of titanate nanosheets. The last weight loss belonged to the complete dehydration of layered titanate. The molar ratio of imidazolium cations calculated from TGA curves (Table 1) presented a declining trend with the increase of length in alkyl chains, while the ratio of interlayer H_2O increased except for that of TiO_2-Emim. Considering that two formula units in 2D unit cell of $Ti_{0.91}O_2$

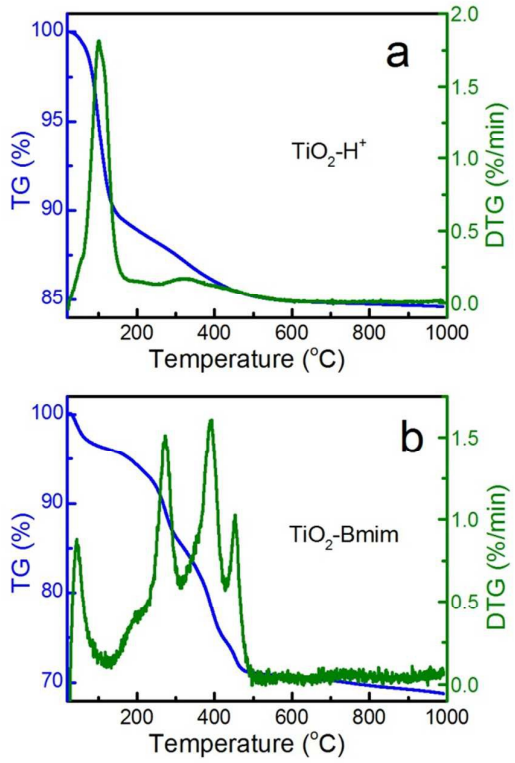

Fig. 7 TGA/DTG curves of a) TiO_2-H^+ and b)TiO_2-Bmim hybrids.

nanosheets have an intrinsic area of 0.112 nm^2 (= 0.3760 × 0.2976),[73] longer alkyl chain occupying more space in the interlayer led to less consumption of corresponding ILs in the hybrid. In another respect, the gallery space of TiO_2-Emim was almost occupied with $Emim^+$ cations, resulting in a substantial loss of free spacing in the interlayer region of composites.

To evaluate the CO_2 uptake capacity of pristine titanate and as-prepared nanocomposites, an IGA experiment was conducted. The IGA analysis (Fig. 8) indicated that TiO_2-H^+ hybrid exhibited the maximum CO_2 adsorption capacity, with 3.0-fold improvement relative to that of protonic bulk precursor, arising from the large planar surface, open pore structures and accessible active sites of restacking aggregates of nanosheets. Unexpectedly, CO_2 uptake capacity of the TiO_2-ILs composites decreased upon substitution of interlayer H^+ with imidazolium cations. It can be speculated that the high ratio of interlayer H_2O molecules played key a role in the high performance of CO_2 uptake. Here we proposed that the absorption of CO_2 by these organic-inorganic layered compounds was principally driven by the water molecules absorbed in the interlayer surface, due to the readily ion-exchangeable and intercalated characteristic of layered structures. CO_3^{2-} and H^+ ions would be formed immediately once CO_2 reacted with the intercalated H_2O. H^+ ions were readily captured by the negative titanate slabs. CO_3^{2-} would interact with imidazolium cations to balance the charge of the system, resulting in the adsorption of CO_2. Therefore, CO_2 uptake capacity of TiO_2-ILs composites decreased compared to that of highly hydrated aggregates flocculating by HCl solution, as the hydratability of substituted imidazolium cations weakened (Table 1).

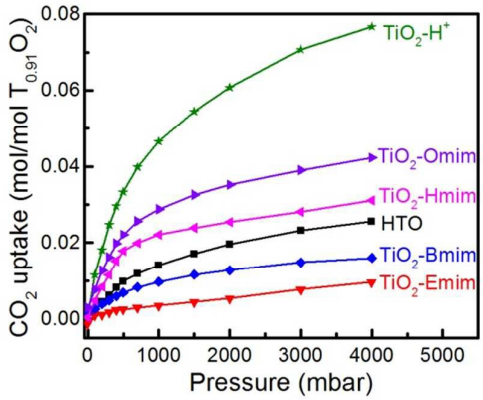

Fig. 8 CO_2 uptake capacity of TiO_2 nanosheets and TiO_2-ILs nanocomposites. The related absorption data was calculated on the basis of $Ti_{0.91}O_2$ unit cell.

Noteworthily, TiO_2-ILs compounds displayed increasing CO_2 absorption capacity with increasing alkyl chain length in imidazolium cations, which can be explained as the synergistically interfacial effects induced by the diverse interactions of ILs and inorganic nanosheets. As mentioned above, ILs with longer carbon chains were less consumed, leading to a lower ratio of ion-exchange and higher ratio of H_2O left in the layered products (Table 1). The results confirmed the absorption mechanism proposed above, in which interlayer H_2O played a pivotal role in CO_2 absorption. For TiO_2-Emim sample, the gallery space and the surface were accommodated with $Emim^+$ cations completely, causing a substantial loss of free spacing for the absorption of CO_2. Consequently, few amounts of CO_2 were absorbed in TiO_2-Emim. Moreover, strength changes in diverse driving forces between the hybridized components can also influence the absorption of CO_2, as the variations not only modified the framework structures, but also altered the basal spacings of the hybrids.

4. Conclusions

Layered TiO_2-ILs nanohybrids were fabricated successfully through an exfoliation-restacking process by interfacially engineering the unique 2D inorganic nanosheets and imidazolium-type ILs. Studies unveiled that interlayer height and ratio of guest species in the nanocomposites could be tuned by the alkyl chain length of ILs, which can in turn affect the performance of CO_2 uptake. The CO_2 uptake capacity of layered compounds decreased upon hybridization with ILs, confirming that the absorption of CO_2 in compounds was driven by intercalated water molecule. The enhanced CO_2 absorption capacity with increasing alkyl chain length in imidazolium cations was attributed to the synergistically interfacial effects induced by water contents and free space in interlayer region, as well as diverse interactions of ILs with inorganic nanosheets. These results provide a better understanding of CO_2 absorption behavior in organic-inorganic heterostructures. The structural integration and interfacial regulation of 2D inorganic nanosheets with ILs will provide a protocol to develop novel layered

nanocomposites for energy and environmental applications, and the relationships of the structure and activity proposed here can shed new light on rationally designing task-specific nanohybrids with improved performance.

Acknowledgements

This work was financially supported by the National Natural Science Foundation of China (No. 21271175, 21127011, 21276261), National Basic Research Program of China (973 program, No. 2014CB239701), International S&T Cooperation Program of China (No. 2014DFA61670), and Instrument and Equipment Research and Development Project of CAS (No. YZ201221).

References

1 Y. Izumi, *Coordin Chem Rev*, 2013, **257**, 171-186.
2 Z.-Z. Yang, L.-N. He, J. Gao, A.-H. Liu and B. Yu, *Energy Environ Sci*, 2012, **5**, 6602.
3 N. MacDowell, N. Florin, A. Buchard, J. Hallett, A. Galindo, G. Jackson, C. S. Adjiman, C. K. Williams, N. Shah and P. Fennell, *Energy Environ Sci*, 2010, **3**, 1645.
4 D. M. D'Alessandro, B. Smit and J. R. Long, *Angew Chem Int Ed Engl*, 2010, **49**, 6058-6082.
5 G. P. Hao, W. C. Li, D. Qian and A. H. Lu, *Adv Mater*, 2010, **22**, 853-857.
6 T. C. Drage, J. M. Blackman, C. Pevida and C. E. Snape, *Energ Fuel*, 2009, **23**, 2790-2796.
7 J. Wei, D. Zhou, Z. Sun, Y. Deng, Y. Xia and D. Zhao, *Adv Funct Mater*, 2013, **23**, 2322-2328.
8 M. Sevilla, P. Valle-Vigón and A. B. Fuertes, *Adv Funct Mater*, 2011, **21**, 2781-2787.
9 M. Sevilla and A. B. Fuertes, *Energy Environ Sci*, 2011, **4**, 1765.
10 X. C. Xu, C. S. Song, J. M. Andresen, B. G. Miller and A. W. Scaroni, *Energ Fuel*, 2002, **16**, 1463-1469.
11 X. Yan, L. Zhang, Y. Zhang, G. Yang and Z. Yan, *Ind Eng Chem Res*, 2011, **50**, 3220-3226.
12 M. B. Yue, Y. Chun, Y. Cao, X. Dong and J. H. Zhu, *Adv Funct Mater*, 2006, **16**, 1717-1722.
13 K. Sumida, D. L. Rogow, J. A. Mason, T. M. McDonald, E. D. Bloch, Z. R. Herm, T. H. Bae and J. R. Long, *Chem Rev*, 2012, **112**, 724-781.
14 R. Banerjee, A. Phan, B. Wang, C. Knobler, H. Furukawa, M. O'Keeffe and O. M. Yaghi, *Science*, 2008, **319**, 939-943.
15 J.-R. Li, Y. Ma, M. C. McCarthy, J. Sculley, J. Yu, H.-K. Jeong, P. B. Balbuena and H.-C. Zhou, *Coordin Chem Rev*, 2011, **255**, 1791-1823.
16 J. Liu, P. K. Thallapally, B. P. McGrail, D. R. Brown and J. Liu, *Chem Soc Rev*, 2012, **41**, 2308-2322.
17 A. C. Sudik, A. R. Millward, N. W. Ockwig, A. P. Cote, J. Kim and O. M. Yaghi, *J Am Chem Soc*, 2005, **127**, 7110-7118.
18 S. Verma, A. K. Mishra and J. Kumar, *Acc Chem Res*, 2010, **43**, 79-91.
19 R. Banerjee, H. Furukawa, D. Britt, C. Knobler, M. O'Keeffe and O. M. Yaghi, *J Am Chem Soc*, 2009, **131**, 3875-+.
20 H. S. Choi and M. P. Suh, *Angew Chem Int Ed Engl*, 2009, **48**, 6865-6869.
21 A. P. Katsoulidis and M. G. Kanatzidis, *Chem Mater*, 2011, **23**, 1818-1824.
22 W. Lu, J. P. Sculley, D. Yuan, R. Krishna, Z. Wei and H. C. Zhou, *Angew Chem Int Ed Engl*, 2012, **51**, 7480-7484.
23 M. G. Rabbani and H. M. El-Kaderi, *Chem Mater*, 2011, **23**, 1650-1653.
24 G.-P. Hao, Z.-Y. Jin, Q. Sun, X.-Q. Zhang, J.-T. Zhang and A.-H. Lu, *Energy Environ Sci*, 2013, **6**, 3740.
25 Q. Sun, Z. Li, D. J. Searles, Y. Chen, G. M. Lu and A. Du, *J Am Chem Soc*, 2013, **135**, 8246-8253.
26 J. Gong, B. Michalkiewicz, X. Chen, E. Mijowska, J. Liu, Z. Jiang, X. Wen and T. Tang, *ACS Sustainable Chemistry & Engineering*, 2014, **2**, 2837-2844.
27 J. L. Gunjakar, I. Y. Kim and S.-J. Hwang, *Eur J Inorg Chem*, 2015, **2015**, 1198-1202.
28 T. W. Kim, I. Y. Kim, T. S. Jung, C. H. Ko and S.-J. Hwang, *Adv Funct Mater*, 2013, **23**, 4377-4385.
29 I. Y. Kim, K. Y. Lee, T. W. Kim and S.-J. Hwang, *Mater Lett*, 2011, **65**, 894-896.
30 A. Zukal, I. Dominguez, J. Mayerova and J. Cejka, *Langmuir*, 2009, **25**, 10314-10321.
31 Q. Wang, J. Luo, Z. Zhong and A. Borgna, *Energy Environ Sci*, 2011, **4**, 42-55.
32 J. L. Gunjakar, I. Y. Kim, J. M. Lee, Y. K. Jo and S. J. Hwang, *J Phys Chem C*, 2014, **118**, 3847-3863.
33 M. Ramdin, T. W. de Loos and T. J. H. Vlugt, *Ind Eng Chem Res*, 2012, **51**, 8149-8177.
34 X. Zhang, X. Zhang, H. Dong, Z. Zhao, S. Zhang and Y. Huang, *Energy Environ Sci*, 2012, **5**, 6668.
35 J. M. Zhang, J. Sun, X. C. Zhang, Y. S. Zhao and S. J. Zhang, *Greenhouse Gases-Science and Technology*, 2011, **1**, 142-159.
36 J. E. Brennecke and B. E. Gurkan, *J Phys Chem Lett*, 2010, **1**, 3459-3464.
37 S. J. Zhang, J. Sun, X. C. Zhang, J. Y. Xin, Q. Q. Miao and J. J. Wang, *Chem Soc Rev*, 2014, **43**, 7838-7869.
38 Y. Zhang and J. Y. G. Chan, *Energy Environ Sci*, 2010, **3**, 408-417.
39 J. E. Bara, T. K. Carlisle, C. J. Gabriel, D. Camper, A. Finotello, D. L. Gin and R. D. Noble, *Ind Eng Chem Res*, 2009, **48**, 2739-2751.
40 C. Cadena, J. L. Anthony, J. K. Shah, T. I. Morrow, J. F. Brennecke and E. J. Maginn, *J Am Chem Soc*, 2004, **126**, 5300-5308.
41 M. B. Shiflett and A. Yokozeki, *Ind Eng Chem Res*, 2005, **44**, 4453-4464.
42 J. L. Anthony, J. L. Anderson, E. J. Maginn and J. F. Brennecke, *J Phys Chem B*, 2005, **109**, 6366-6374.
43 M. S. Shannon, M. S. Hindman, S. P. O. Danielsen, J. M. Tedstone, R. D. Gilmore and J. E. Bara, *Science China-Chemistry*, 2012, **55**, 1638-1647.
44 C. P. Mehnert, R. A. Cook, N. C. Dispenziere and M. Afeworki, *J Am Chem Soc*, 2002, **124**, 12932-12933.
45 H. Li, P. S. Bhadury, B. Song and S. Yang, *RSC Advances*, 2012, **2**, 12525.
46 J. Le Bideau, L. Viau and A. Vioux, *Chem Soc Rev*, 2011, **40**, 907-925.
47 F. R. Eirich, *Applied polymer symposia*, 1984, **39**, 93-102.
48 B. Pukánszky, *Eur Polym J*, 2005, **41**, 645-662.
49 M. V. Fedorov and A. A. Kornyshev, *Chem Rev*, 2014, **114**, 2978-3036.
50 R. An, Y. D. Zhu, N. H. Wu, W. L. Xie, J. W. Lu, X. Feng and X. H. Lu, *ACS Appl Mater Interfaces*, 2013, **5**, 2692-2698.
51 J. Shi, *Chem Rev*, 2013, **113**, 2139-2181.
52 J. L. Gunjakar, I. Y. Kim, J. M. Lee, Y. K. Jo and S.-J. Hwang, *The Journal of Physical Chemistry C*, 2014, **118**, 3847-3863.
53 W. A. England, J. E. Birkett, J. B. Goodenough and P. J. Wiseman, *J Solid State Chem*, 1983, **49**, 300-308.
54 T. Sasaki, S. Nakano, S. Yamauchi and M. Watanabe, *Chem Mater*, 1997, **9**, 602-608.
55 T. Sasaki, F. Kooli, M. Iida, Y. Michiue, S. Takenouchi, Y. Yajima, F. Izumi, B. C. Chakoumakos and M. Watanabe, *Chem Mater*, 1998, **10**, 4123-4128.
56 T. Gao, H. Fjellvag and P. Norby, *Chem Mater*, 2009, **21**, 3503-3513.

57 T. Gao, H. Fjellvag and P. Norby, *J Phys Chem B*, 2008, **112**, 9400-9405.
58 W. Zheng, X. Liu, Z. Yan and L. Zhu, *ACS Nano*, 2009, **3**, 115-122.
59 J. Zhu, J. G. Wang, F. J. Lv, S. X. Xiao, C. Nuckolls and H. X. Li, *J Am Chem Soc*, 2013, **135**, 4719-4721.
60 I. Y. Kim, Y. K. Jo, J. M. Lee, L. Wang and S.-J. Hwang, *The Journal of Physical Chemistry Letters*, 2014, **5**, 4149-4161.
61 T. Sasaki, M. Watanabe, Y. Michiue, Y. Komatsu, F. Izumi and S. Takenouchi, *Chem Mater*, 1995, **7**, 1001-1007.
62 W. Fan, Q. Zhang, W. Deng and Y. Wang, *Chem Mater*, 2013, **25**, 3277-3287.
63 T. Sasaki, Y. Ebina, Y. Kitami, M. Watanabe and T. Oikawa, *J Phys Chem B*, 2001, **105**, 6116-6121.
64 H. Hu, J. C. Martin, M. Xiao, C. S. Southworth, Y. Z. Meng and L. Y. Sun, *J Phys Chem C*, 2011, **115**, 5509-5514.
65 Y. Ide, Y. Nakasato and M. Ogawa, *J Am Chem Soc*, 2010, **132**, 3601-3604.
66 R. Z. Ma, K. Fukuda, T. Sasaki, M. Osada and Y. Bando, *J Phys Chem B*, 2005, **109**, 6210-6214.

67 A. Takagaki, C. Tagusagawa, S. Hayashi, M. Hara and K. Domen, *Energy Environ Sci*, 2010, **3**, 82-93.
68 H. Meng, X.-W. Chen and J.-H. Wang, *J Mater Chem*, 2011, **21**, 14857-14863.
69 C.-C. Han, S.-Y. Ho, Y.-P. Lin, Y.-C. Lai, W.-C. Liang and Y.-W. Chen-Yang, *Micropor Mesopor Mat*, 2010, **131**, 217-223.
70 T. Gao, H. Fjellvåg and P. Norby, *J Mater Chem*, 2009, **19**, 787-794.
71 L. Wang and T. Sasaki, *Chem Rev*, 2014, **114**, 9455-9486.
72 H. Hu, J. C. Martin, M. Zhang, C. S. Southworth, M. Xiao, Y. Meng and L. Sun, *Rsc Advances*, 2012, **2**, 3810-3815.
73 L. Li, R. Ma, Y. Ebina, K. Fukuda, K. Takada and T. Sasaki, *J Am Chem Soc*, 2007, **129**, 8000-8007.

TOC abstract and short summary

Interfacial properties of layered TiO_2-ILs hybrids could be tuned by the alkyl chain length in imidazolium cations, which can in turn affect the performance of CO_2 uptake.